First-Principles Thermochemistry for Silicon Species in the Decomposition of Tetraethoxysilane

Weerapong Phadungsukanan, Shraddha Shekar, Raphael Shirley, Markus Sander, Richard H. West, and Markus Kraft*

Department of Chemical Engineering and Biotechnology, University of Cambridge, New Museums Site, Cambridge, U.K.

Received: June 11, 2009; Revised Manuscript Received: June 24, 2009

Tetraethoxysilane (TEOS) is used as a precursor in the industrial production of silica nanoparticles using thermal decomposition methods such as flame spray pyrolysis (FSP). Despite the industrial importance of this process, the current kinetic model of high-temperature decomposition of TEOS to produce intermediate silicon species and eventually form amorphous silica (α-SiO_2) nanoparticles remains inadequate. This is partly due to the fact only a small proportion of the possible species is considered. This work presents the thermochemistry of practically all of the species that can exist in the early stages of the reaction mechanism. In order to ensure that all possible species are considered, the process is automated by considering all species that can be formed from the reactions that are deemed reasonable in the standard ethanol combustion model in the literature. Thermochemical data for 180 species (over 160 of which have not appeared in the literature before) are calculated using density functional theory with two different hybrid functionals, B3LYP and B97-1. The standard enthalpy of formation ($\Delta_f H^\circ_{298.15K}$) values for these species are calculated using isodesmic reactions. It is observed that internal rotation may be important because the barriers to rotation are reasonably low. Comparisons are then made between the rigid rotor harmonic oscillator approximation (RRHO) and the RRHO with some of the vibrational modes treated as hindered rotors. It is found that full treatment of the hindered rotors makes a significant difference to the thermochemistry and thus has an impact on equilibrium concentrations and kinetics in this system. For this reason, all of the species are treated using the hindered rotor approximation where appropriate. Finally, equilibrium calculations are performed to identify the intermediates that are likely to be most prevalent in the high-temperature industrial process. Particularly, $Si(OH)_4$, $SiH(OH)_3$, $SiH_2(OH)_2$, $SiH_3(OH)$, $Si(OH)_3(OCH_3)$, $Si(OH)_2(OCH_3)_2$, the silicon dimers $(CH_3)_3$-$SiOSi(CH_3)_3$ and SiH_3OSiH_3, and the smaller hydrocarbon species CH_4, CO_2, C_2H_4, and C_2H_6 are highlighted as the important species.

Introduction

Silica nanoparticles are widely used as a support for functional materials. Silica is inherently thermally stable, which makes it useful as a substrate for active substances such as expensive metals and polymers. Silica nanoparticles have traditionally been used in ceramics, catalysis, chromatography, and chemomechanical polishing.[1] Recently, there has been increased interest in potential applications of silica nanoparticles in the biomedical sector, for drug delivery and biosensing applications.[2] The combustion synthesis of silica nanoparticles with tetraethoxysilane as a precursor is a well-established industrial process. It is well-known that the properties of silica nanoparticles depend on particle size and primary particle size distribution.[3] In order to control particle size and to understand high-purity material synthesis processes such as chemical vapor deposition (CVD), a detailed kinetic model of the TEOS decomposition mechanism is required. In the system studied in this work, TEOS undergoes thermal decomposition at high temperatures (1100−1500 K) and at atmospheric pressure to produce silica nanoparticles. The overall stoichiometry for this decomposition process is

$$Si(OC_2H_5)_4 \rightarrow SiO_{2(\text{silica nanoparticles})} + \text{Products} \quad (1)$$

Previous attempts to understand this process have been made by Chu et al.[4] and Herzler et al.,[5] who describe the formation of silicon dioxide molecules based on unimolecular reactions of tetraethoxysilane and its sequential products. Chu et al.[4] suggested a six-center molecular decomposition process of the ethoxy groups to be responsible for the major decomposition of TEOS, with the generation of one ethylene and one ethanol per two decompositions of an ethoxy group from a TEOS molecule. Later, Herzler et al.[5] studied the decomposition of TEOS and other molecules in a single-pulse shock tube experiment in a temperature range between 1160 and 1285 K and at a pressure of about 150 kPa (1.5 bar); the product yield studies suggested a different decomposition mechanism than that of Chu et al.;[4] a more complicated four-center 1,2-elimination reaction was considered as an alternative tetraethoxysilane decomposition reaction. Though the kinetics proposed by Herzler et al.[5] adequately describes the primary irreversible reactions of the system, it fails to explain the absence of any silicon compound detection in the experiment. An accurate kinetic model is a necessary requirement of any model of the particulate processes involved in the formation of SiO_2 nanoparticles.[6−9]

The aim of this work is to provide the thermochemical properties for the set of all possible closed-shell and radical silicon species generated from the decomposition of TEOS. The

* To whom correspondence should be addressed.

10.1021/jp905494s CCC: $40.75
Published on Web 07/15/2009

thermodynamic properties of some of such chemical species involving Si−O−C−H bonds were calculated by Ho and Melius[10] from MP4 calculations with bond additivity corrections (BAC). However, complete analysis of the TEOS system leads us to believe that more species than those provided by Ho and Melius[10] might be involved in the reaction mechanism.

In order to produce an exhaustive pool of species that are likely to participate in the course of TEOS decomposition, consideration of all possible species has been automated using a script written in Perl. Thermodynamic properties have been determined using density functional theory (DFT) and principles of statistical mechanics. Equilibrium calculations can then be performed as a first attempt to identify the important species in the reaction mechanism and to characterize the nucleation process.

This work also examines the effect that internal rotors have on the thermochemistry of silicon molecules using a one-dimensional hindered rotor approximation. The torsional barriers of CH_3 rotors in many silicon compounds were found to be similar irrespective of the chemical environment of the rotor. The classical hindered rotor partition function has been used to treat all of the CH_3 and SiH_3 rotors in the high-temperature regime. The calculated thermodynamic properties of some reference species, such as $Si(OH)_3(OC_2H_5)$, $SiH_3(OC_2H_5)$, $Si(OH)_3(OCH_3)$, $Si(OH)_2(OCH_3)_2$, $Si^{\bullet}(OH)_2(OCH_3)$, and $Si(OH)_3(OC^{\bullet}H_2)$, are in good agreement with those computed by Ho and Melius,[10] which were later revised with hindered rotor corrections by Sandia National Laboratory.

Methods Section

Automatic Molecular Structure Generation. In the absence of an accurate mechanism describing the decomposition of TEOS, we hypothesize that each of the four ethoxy functional groups (OCH_2CH_3) attached to the Si atom can break down into smaller species in the same way as for the ethanol reactions as proposed by Marinov et al.[11] For the automatic generation of silicon species generated from decomposed TEOS, each of the four ethoxy branches is systematically changed in order to produce every possible permutation of ligands. Some of these species have been previously studied by Ho et al.[10] using MP2/MP4 and BAC, who manually worked their way through possible geometries. The branches can be in a number of different states; for completeness, we consider all possible branch types. It is anticipated that a large number of these species will be unrealistic or extremely short-lived. The automation makes this possible and indeed desirable since we can be confident that no important species will be neglected. Any irrelevant species may then be weeded out by observing the equilibrium composition. Some species did not converge under the automated quantum calculations. These were then rerun using a larger number of iterations or by changing the starting geometries until they could be made to converge. The branch ends that are considered are

• **Step 1: Radical species.** Radicals are produced by removing either the H atom on the carbon end, the CH_3, the CH_2CH_3, or the OCH_2CH_3 on each of the ethoxy branches independently, giving a set of 256 species in the preliminary step. Due to the tetragonal symmetry of the molecule, a number of the species generated are not unique. In order to remove the duplicates, an International Chemical Identifier (InChI) name, which can uniquely identify molecules of the same connectivity, is assigned to each species. Duplicate species can then be automatically removed from the set by simply comparing the InChI names using a simple Python script. Unfortunately, InChI strings cannot distinguish between left- and right-handed chiral molecules; therefore, a small number of unique species will be removed. Thermodynamic properties of chiral species are considered to be identical to those of its original. The OpenBabel[12,13] software package is used to convert the molecular connectivity to an InChI name. This procedure results in 64 unique radical species.

• **Step 2: Hydrogen additions.** A radical species generated in the first step may contain one to four radical sites. Molecules with more than one radical site are deemed highly unstable and are not considered in the present work. Therefore, the radical sites are replaced by hydrogen atoms to form nonradical and single-radical site species. A nonradical species is obtained if all radical sites are replaced by hydrogen atoms. Equally, it is possible to leave any one of the radical sites unchanged to form a single-radical site species. Again, duplicates are removed using InChI names.

• **Step 3: Species with C═C double bonds.** The species generated in step 1 can have an OCH_2CH_2 branch replaced by an $OCH{=}CH_2$ branch. This is easily done by removing the hydrogens that are connected to the terminal and penultimate carbon atoms; the subsequent electronic minimization will then find that the lowest-energy state is that with a double bond and correct the bond lengths. For species with more than one OCH_2CH_2 branch, all possible combinations of replacements are applied. Hydrogen addition and duplication removal steps are also performed on this new set.

The total number of silicon species is the sum of those produced by steps 1−3, including all single-radical site species and TEOS. The above steps are implemented in a Perl script, generating a total of 180 possible silicon species. A number of the species generated are shown in Figure 1.

Quantum Calculations. Quantum calculations are performed on the 180 generated species with DFT functionals using the Gaussian 03 software package.[14] Geometries are optimized and harmonic frequencies calculated using B3LYP[15] and B97-1[16] functionals. The basis set used for all reported calculations is 6-311+G(d,p), which assumes Slater-type orbitals.[14] The 6-311+G(d,p) consists of the 6-311G basis set[17] for first-row atoms, the McLean-Chandler (12s,9p) (621111,52111) basis sets[18] for second-row atoms, and additional extra valence functionals, polarization functionals, and diffuse functionals for second-row atoms. This basis set contains at least triple-ζ basis sets for second-row atoms, as recommended by McLean et al.[18] This 6-311+G(d,p) basis set should be large enough for the basis set truncation error to be smaller than the inherent errors of the DFT functional itself.[19] Table 1 shows literature values for the enthalpy of formation, which will be used in correcting errors in the DFT calculations using the method of isodesmic reactions as described by West et al.[20]

Tight convergence criterion is used for the self-consistent field calculations, and orbital symmetry constraints are lifted for all species. The pruned (99,590) integral grid is used, as recommended,[14] for molecules containing many tetrahedral centers and for increasing the numerical accuracies of very low frequency modes. However, the lowest-energy conformers of many silicon species are still very difficult to determine because of the existence of the many local minima around tetrahedral centers on the potential energy surface. Thus, the geometry of TEOS, which is used as the starting point for smaller silicon species, is carefully optimized to achieve the lowest-energy structure.

A comparative study of the DFT functionals, B3LYP and B97-1, enables us to check the validity of the calculations from agreement between the two functionals; any remaining errors must then be due to inherent problems with DFT. In the case of B3LYP, the exchange−correlation energy functional in the

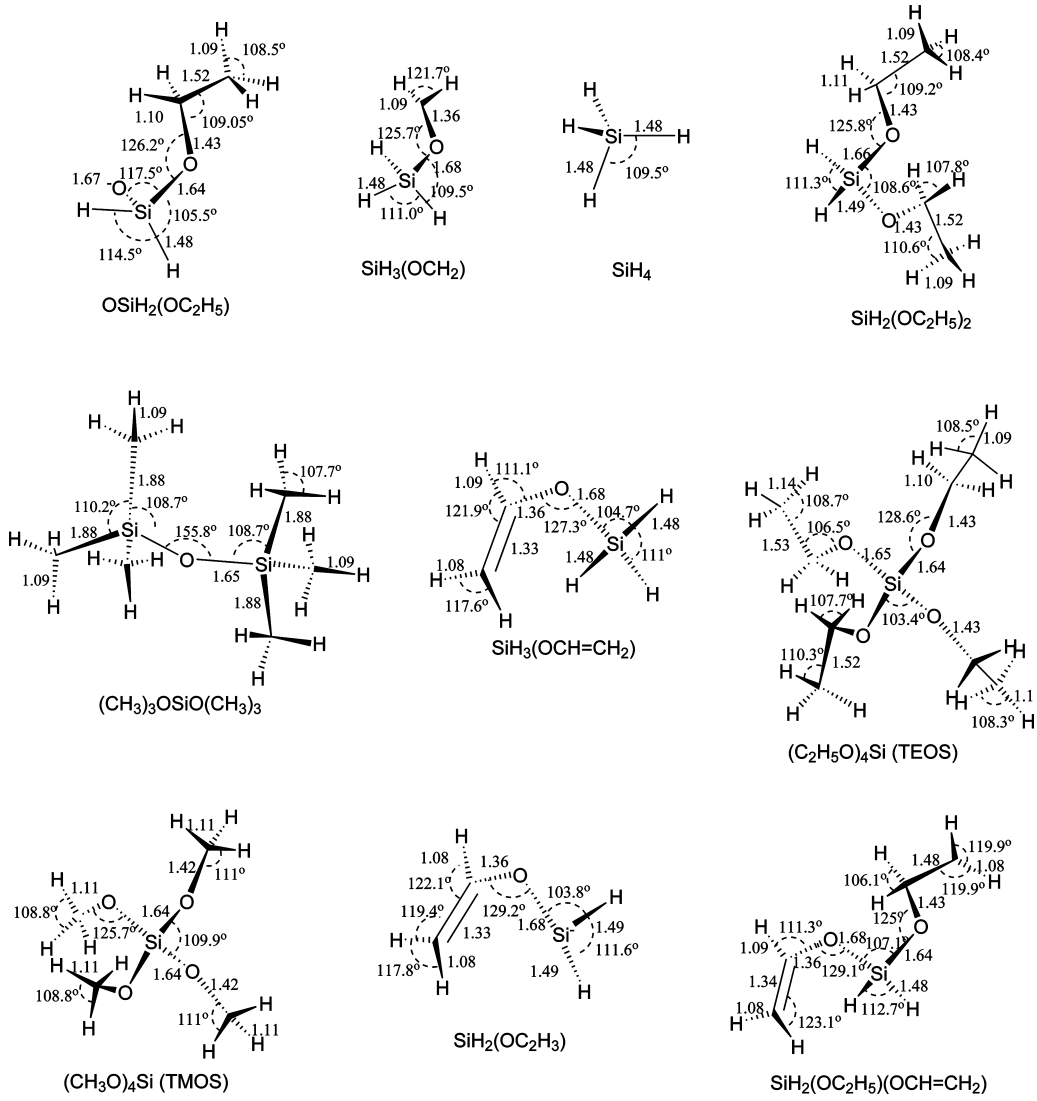

Figure 1. Molecular geometries after optimization with B97-1/6-311+G(d,p); bond lengths are in Ångströms, and unlabeled atoms are carbon. The bold wedged bonds and the hashed wedged bonds indicate bonds coming out of the plane and going into the plane, respectively.

DFT calculation uses the approximation of Lee−Yang−Parr.[21] The B97-1 hybrid functional[16,22] is a combination of a nine-term continuum expansion and a fraction of exact orbital exchange, whose optimal expansion parameters are determined through a fit to molecular thermochemical data.[23] Boese[19] recommends B97-1 as the best choice for DFT calculations.

Internal Rotors. The largest contributions to the absolute entropy and other thermodynamic properties are from the low-frequency vibrational modes. In silicon species, several of the low-frequency modes correspond to internal rotors where the potential energy surface is better described by a sinusoidal internal rotation potential rather than a harmonic vibrational potential. Treating internal rotation properly becomes especially important for creating accurate thermochemistry data. In this work, CH_3 and SiH_3 rotors are of interest because the rotational symmetries of these rotors allow the torsional potential barriers, $V(\phi)$, to be described by single cosine functions

$$V(\phi) = \frac{V_0}{2}(1 - \cos(n\phi)) \qquad (2)$$

where ϕ is the dihedral angle of the torsion motion and n is the symmetry number of the rotor for the number of indistinguishable minima on the potential surface of the rotor, that is, three for CH_3 and SiH_3. For a more complicated potential such as for nonsymmetrical tops, the m term truncated Fourier expansion may be used to represent the potential.[24]

The methods used to obtain high-accuracy torsional barriers and reduced moments of inertia have been discussed by several researchers.[24−26] The dihedral angle of the rotor is rotated from 0 to 360° at 12° intervals. This dihedral angle is constrained, allowing the rest of molecular structure parameters to be fully relaxed. The differences between the total energy of each conformation and that of the most stable optimized structure define the potential energy as a function of the dihedral angle. The results of calculations at the B3LYP/6-311+G(d,p) and B97-1/6-311+G(d,p) levels are shown in Table 2 and Figure 2. The entire molecule is allowed to relax at each angle of rotation (while constraining that angle) because the torsional barrier is coupled to the rotor's chemical environment.

In the present work, the internal rotors of all silicon species are treated using the popular 1-D hindered rotor (1-DHR) approximation.[24,27] The hindered rotor form of the Schrödinger equation (eq 3) is based on the assumption that the solution of the hindered internal rotor is separable from those of other rotors and any overall rotation.

$$\frac{-\hbar^2}{2I_r}\frac{d^2\psi}{d\phi^2} + (V(\phi) - \varepsilon)\psi = 0 \quad (3)$$

$$q^{\text{class hind}} = \frac{1}{n}\left(\frac{2\pi I_r k_B}{\hbar^2}T\right)^{1/2}\int_0^{2\pi/n} e^{-V_0(1-\cos n\phi)/2k_BT}d\phi \quad (4)$$

For molecules with multiple rotors, the torsional potential and the reduced moment of inertia of a particular rotor require consideration of coupling to other rotors in the molecule. Pitzer et al.[28] have shown that these couplings can be accounted for using Pitzer's formulas to calculate the reduced moment of inertia. The current conventional notation for these formulas was introduced by East et al.[29] for ease of understanding. The reduced moments of inertia, I_r, are computed using Pitzer's formulas about the axis that passes through the centers of mass of both the rotating group and the rest of the molecule, $I^{(2,3)}$.

The vibrational frequencies and internal rotation axes that correspond to the internal rotations are identified by looking at the motions of all atoms according to the RRHO. This is done by looking for a large dihedral angle movement of the rotating group while bond stretching, bending, and out-of-plane bending motions of the rest of the molecule remain almost stationary. The partition functions of those corresponding frequencies are then replaced by the internal rotor partition function. Solving the rotational Schrödinger equation numerically for energy levels involves computing complicated numerical solutions. Instead, we used the classical approximation to the hindrance partition function, eq 4

McClurg et al.[30] have shown that this partition function performs remarkably well in the high-temperature limit like those conditions that occur in the industrial reactor. This is because the number of accessible quantum states becomes very large at high temperature and begins to approximate a continuum. The summation over all of the energy states in the partition function can then be approximated by the integral over phase space. The treatment of rotor−rotor coupling of the hindered potential surface was illustrated by East et al.[29] These cross-term potentials are less than 0.01 kcal/mol, and we have neglected them in species with multiple internal rotors, that is, species with multiple methyl groups.

Thermochemistry Calculation and Equilibrium Composition. The standard enthalpy of formation at 0 K, $\Delta_f H^\circ_{0K}$, can be determined by subtracting the energy of the species from the energy of its elements in their standard states as calculated from a DFT calculation. However, there are large errors associated with total electronic energies from DFT, and this method leads to poor values of $\Delta_f H^\circ_{0K}$. Here, $\Delta_f H^\circ_{0K}$ is calculated using the method of isodesmic reactions as used by West et al. for titanium oxychloride species.[20] In an isodesmic reaction, the type of bonds formed in the products are the same as those which are broken in the reactants. An isodesmic reaction is chosen to relate

TABLE 1: Literature Standard Enthalpy of Formation, $\Delta_f H^\circ_{298.15K}$, and Calculated Electronic Energies at B97-1/6-311+G(d,p) and B3LYP/6-311+G(d,p) versus MP4(SDTQ)

species	$\Delta_f H^\circ_{298.15K}$(kcal/mol)	ref	electronic energies (hartrees)		
			MP4(SDTQ)[a]	B97-1	B3LYP
$\ddot{C}H_2$	388.28 ± 5.77	Melius[a]	−39.037812	−39.135089	−39.166080
$C^{\bullet}H_3$	146.02 ± 4.94	Melius[32]	−39.714719	−39.832163	−39.855167
CH_4	−74.89 ± 4.18	Allendorf[a]	−40.388610	−40.511179	−40.533927
$CH_2{=}CH_2$	51.46 ± 4.18	Allendorf[a]	−78.353058	−78.581437	−78.615513
$CH_3C^{\bullet}H_2$	120.50 ± 5.40	Melius[32]	−78.914811	−79.148310	−79.185020
CH_3CH_3	−87.03 ± 4.31	Sandia[a]	−79.584024	−79.819722	−79.856544
$C^{\bullet}H_2OH$	−20.50 ± 4.48	Melius[a]	−114.751281	−115.060771	−115.102488
$O{=}CHCH_3$	−161.50 ± 4.39	Allendorf[a]	−153.417858	−153.829593	−153.882147
$CH_3CH_2O^{\bullet}$	−2.09 ± 4.44	Melius[a]	−153.945992	−154.367095	−154.251414
CH_3OCH_3	−183.26 ± 6.23	Melius[a]	−154.598322	−155.019655	−155.077044
C_2H_5OH	−238.91 ± 4.23	Melius[a]	−154.614399	−155.038409	−155.094967
$(CH_3CH_2)O(CH_2CH_3)$	−252.67 ± 2.01	Pedley[33]		−233.648699	−233.734152
$O^{\bullet}H$	38.95 ± 4.23	NIST-JANAF		−75.735621	−75.762337
H_2O	−241.84 ± 4.18	Cox[34]	−76.230814	−76.431169	−76.458464
$O{=}CH_2$	−108.37 ± 4.18	Melius[a]	−114.206279	−114.503529	−114.541756
$SiH_3(O^{\bullet})$	20.08 ± 4.81	Allendorf[a]	−365.768988	−366.434921	−366.514635
$SiH_3(OC_2H_5)$	−276.56 ± 4.18	Ho[10]	−444.840821	−445.735503	−445.845053
$SiH(OH)_3$	−981.57 ± 6.90	Allendorf[35]	−516.665457	−517.700877	−517.822827
$Si^{\bullet}(OH)_2(OCH_3)$	−740.99 ± 4.23	Ho[10]	−555.187981	−556.334721	−556.470223
$Si(O^{\bullet})(OH)_3$	−1033.87 ± 13.6	Allendorf[35]	−591.080624	−592.290404	−592.431993
$Si(OH)_4$	−1342.23 ± 13.9	Allendorf[35]	−591.772791	−592.988897	−593.131180
$Si^{\bullet}(OH)(OCH_3)_2$	−706.68 ± 4.35	Ho[10]	−594.368887	−595.625923	−595.776426
$Si(O^{\bullet})(OH)_2(OCH_3)$	−996.21 ± 14.5	Ho[10]	−630.260421	−631.581849	−631.733105
$Si(OH)_3(OC^{\bullet}H_2)$	−1112.94 ± 17.0	Ho[10]	−630.290120	−631.615044	−631.771792
$Si(OH)_3(OCH_3)$	−1305.41 ± 14.4	Ho[10]	−630.952798	−632.279815	−632.437066
$(SiH_3)O(SiH_3)$	−331.79 ± 8.16	Sandia[a]	−656.686243	−657.833237	−657.967161
$Si(OH)_2(OCH_3)_2$	−1259.38 ± 15.3	Ho[10]	−670.129440	−671.567103	−671.739213
$Si(OH)_3(OC_2H_5)$	−1340.97 ± 13.3	Ho[10]	−670.157286	−671.595554	−671.766701
$O{=}Si^{\bullet}OH$	−310.03 ± 6.74	Allendorf[35]	−439.690209	−440.527830	−440.623471
$O{=}SiH(O^{\bullet})(OH)$	−489.95 ± 20.9	Allendorf[35]	−514.734582	−515.760450	−515.877357
$O{=}SiH(OH)(OCH_3)$	−772.78 ± 26.8	Ho[10]	−555.187981	−555.746704	−555.879357
$O{=}SiH(OCH_3)_2$	−735.55 ± 27.3	Ho[10]	−593.790890	−595.038242	−595.186008

[a] Online gas-phase resources provided by HiTempThermo, Sandia National Laboratories.

TABLE 2: Torsional Barriers of CH_3 and SiH_3 Rotors Calculated Using the B3LYP/6-311+G(d,p) and B97-1/6-311+G(d,p) Levels of Theory and the Reduced Moment of Inertia Calculated Using Pitzer's Formula

		barriers (kJ/mol)			I_r (amu Bohr^2)		
species	rotor[b]	B97-1	B3LYP	lit.	$I^{(1,n)}$	$I^{(2,n)}$	$I^{(3,n)}$
C_2H_5OH	CH_3	13.14	13.22	12.85[40]−14.31[a]	10.35	9.40	9.40
$SiH_2(OH)(OCH_3)$	CH_3	1.76	1.80	−	11.42	11.22	10.87
$SiH(OH)_2(OCH_3)$	CH_3	1.92	2.01	−	11.42	11.23	11.01
$Si(OH)_3(OCH_3)$	CH_3	1.88	1.97	1.88[a]	11.44	11.32	11.20
$SiH_3(OCH_3)$	CH_3	2.89	2.80	−	11.42	10.90	9.60
	SiH_3	4.90	4.69	−	21.25	17.25	13.80
$SiH_3(OC_2H_5)$	CH_3	13.31	13.22	17.20[a]	11.40	11.37	11.35
	SiH_3	4.81	4.90	4.90[a]	20.72	16.98	13.43
$Si(OC_2H_5)_4$	$CH_3^{(1)}$	13.31	13.22	−	11.36	11.34	11.33
	$CH_3^{(2)}$	13.31	13.22		11.36	11.34	11.33
	$CH_3^{(3)}$	13.31	13.22		11.36	11.34	11.33
	$CH_3^{(4)}$	13.31	13.22		11.36	11.34	11.33
$Si(OC_2H_5)_4$*	$CH_3^{(1,2)}$	13.31	13.22	−	11.42	11.34	11.33
$Si(OCH_3)_4$	$CH_3^{(1)}$	1.84	1.92	−	11.42	11.40	11.36
	$CH_3^{(2)}$	1.88	1.97		11.42	11.40	11.36
	$CH_3^{(3)}$	1.88	1.97		11.42	11.40	11.36
	$CH_3^{(4)}$	1.84	1.92		11.42	11.40	11.36
$Si(OCH_3)_4$*	$CH_3^{(1,2)}$	1.92	2.01	−	11.44	11.39	11.36

[a] Online gas-phase resources provided by HiTempThermo, Sandia National Laboratories. [b] (*j*): Torsional barrier of the rotor *j* in the molecule. Numbering of the rotor is arbitrary. (*i*,*j*): Torsional barrier of the rotor *j* while keeping rotor *i* at its maximum.

the species with unknown enthalpy to species with similar bonds, whose enthalpies are known in the literature. In this work, we have tried to relate all of the species using isodesmic reactions to known species from the literature, shown in Table 1. For this method to be applicable, it is important to have a large pool of species with accurate known enthalpies in order to be able to find isodesmic reactions for most of the unknown species. Ho, Allendorf, and Melius have performed ab initio electronic structure calculations and bond additivity corrections (BAC) with MP2/MP4 calculations to calculate the enthalpy of formation of some species containing Si−O−H and Si−O−C−H bonds. The enthalpy of formation as calculated by Ho et al. agrees, within 0.05 J/mol, with data obtained from the NIST database for the few small species where experimental values are available,[31] providing evidence for the validity of values calculated by Ho et al. As there are only a few experimental values available for species that include Si, we extended the experimental values using the thermochemistry calculated by Ho and Melius as a starting point.[10] Table 1 lists $\Delta_f H^\circ_{298.15K}$ for all species known in the literature and compares their electronic energies resulting from highly accurate MP4 calculations against the values calculated in the current work.

Analysis of equilibrium enables us to identify important intermediate species that play an important role in the reaction mechanism. In the current work, equilibrium concentrations are calculated using the open source software Cantera.[36] The thermochemistry data for each species are represented in standardized form as a NASA polynomial[37] which is compatible with the Cantera[36] and CHEMKIN[38] reaction modeling codes. Using these fitted polynomials for $C_p(T)$, $H°(T)$, and $S°(T)$, the equilibrium composition is calculated as a function of temperature.

Results and Discussion

Thermodynamic properties for smaller silicon species have been previously computed using MP2/MP4 calculations with bond additivity corrections (BAC) by Ho et al.,[10] and these results compare well with our calculated values as listed in Table 3. The intermediate results such as the optimized structures, vibrational frequencies, torsional barriers, and rotational constants of all species, which are required for calculating the ideal gas thermodynamic properties, such as S and C_p, are also included as Supporting Information.

Geometries and Frequencies. The molecular geometries of all of the molecules have been optimized at the B3LYP/6-311+G(d,p) and B97-1/6-311+G(d,p) levels of theory, and their bond lengths and torsional angles were calculated. The resultant optimized structures of some important species are shown in Figure 1. For this work, the thermodynamic properties of all species are reported for the lowest-energy structures.

The geometry optimization routine is followed by frequency analysis. The vibrational frequencies for the complete species set as computed by the frequency analysis in Gaussian 03 using the B97-1/6-311+G(d,p) and B3LYP/6-311+G(d,p) levels are provided in the Supporting Information.

Internal Rotors. The calculated torsional barrier heights of CH_3 and SiH_3 rotors of C_2H_5OH (*trans*-ethanol), $SiH_2(OH)(OCH_3)$, $SiH(OH)_2(OCH_3)$, $Si(OH)_3(OCH_3)$, $SiH_3(OCH_3)$, $SiH_3(OC_2H_5)$, $Si(OCH_3)_4$, and $Si(OC_2H_5)_4$ are shown in Table 2. Figure 2 shows the barrier as a function of the dihedral angle at every 12° interval. All potentials are almost symmetric with three-fold barrier symmetry and perfectly fit to a single cosine function given in eq 2. The barrier heights of C═C in ethanol at the B97-1/6-311+G(d,p) and B3LYP/6-311+G(d,p) levels of theory are 13.14 and 13.22 kJ/mol, respectively. These results are comparable to 13.93 and 15.15 kJ/mol from experiment,[39,40] with small underestimation as reported by Viruela et al.[41] that DFT calculations underestimate the torsional barrier in most cases. The above data show the barrier heights for the methyl rotors as 13.22 and 13.30 kcal/mol for B97-1 and B3LYP, respectively, in any ethoxyl group of TEOS. These are similar to those of ethanol calculated at the same level of theory. The same barrier heights are observed for methyl rotors in any silicon species containing any number of ethoxyl groups. This is mostly because the electronic structures of ethanol and the ethoxyl group will be very similar. For the methyl rotor about the C−O bond, we find that the barrier heights of $SiH_3(OCH_3)$ are 2.89 and 2.81 kJ/mol with B97-1/6-311+G(d,p) and B3LYP/6-311+G(d,p), respectively, while the barriers for other silicon species containing more than one oxygen atom, regardless of the functional group attached to the other oxygens, are around

TABLE 3: Ideal Gas Thermodynamic Properties of Some Silicon Species Compared to Ho and Melius's[10] BAC-MP4 Calculations

				C_p (J/mol)					
species	con.[a]	$\Delta_f H^\circ_{298.15K}$ (kJ/mol)	$S_{298.15K}$ (J/mol)	300	500	800	1000	1500	2000
$SiH_3(O^\bullet)$	TVR		249.61	51.92	68.35	83.20	89.47	98.15	102.08
	lit.	20.08 ± 4.81	256.56	52.52	68.77	83.73	89.97	98.50	102.31
SiH_4	TVR	48.80 ± 10.07	204.56	42.89	58.82	76.13	83.93	95.05	100.17
	lit.	34.31 ± 4.18	204.59	43.45	59.90	77.56	85.28	95.98	100.79
$O{=}Si(O^\bullet)(OH)$	TVR		293.80	70.56	84.28	92.93	95.91	100.43	102.98
	lit. + IR	−489.95 ± 20.92	297.31	70.50	83.27	90.57	93.12	97.14	99.43
$Si(O^\bullet)(OH)_3$	TVR		333.18	107.11	132.03	147.25	152.97	162.95	169.27
	lit. + IR	−1033.87 ± 13.60	342.75	104.94	125.19	137.76	142.91	152.29	158.18
$Si(OH)_3(OC^\bullet H_2)$	TVR		373.32	136.93	171.95	197.46	208.00	225.87	236.44
	lit. + IR	−1112.94 ± 16.99	384.64	136.85	169.46	192.30	201.61	216.84	242.99
$Si(OH)_4$	TVR		335.04	114.63	143.95	162.07	169.08	181.75	189.94
	lit. + IR	−1342.23 ± 13.85	342.54	115.77	138.13	151.25	156.96	168.18	175.54
$Si(OH)_3(OC_2H_5)$	TVR		395.51	145.95	199.11	245.73	265.83	298.15	315.91
	IR		8.11	9.65	9.47	7.74	6.82	5.55	4.99
	TVR + IR		403.62	155.60	208.58	253.47	272.65	303.70	320.90
	TVR + f_r		406.78	153.92	207.30	253.99	274.11	306.45	324.21
	lit. + IR	−1340.97 ± 13.26	412.54	152.74	202.47	247.76	267.35	298.44	315.06
$SiH_3(OC_2H_5)$	TVR		310.63	81.37	125.81	172.70	193.62	224.94	240.38
	IR		17.85	19.46	18.54	14.85	13.10	10.76	9.77
	TVR + IR		328.48	100.83	144.35	187.55	206.72	235.70	250.15
	TVR + f_r		330.60	96.79	141.99	189.16	210.14	241.51	256.98
	lit. + IR	−276.56 ± 4.18	334.26	97.55	140.09	184.75	204.43	233.38	247.38
$Si(OH)_3(OCH_3)$	TVR		361.74	125.52	165.03	198.22	212.43	235.73	248.91
	IR		14.72	5.32	4.61	4.34	4.27	4.21	4.19
	TVR + IR		376.46	130.84	169.63	202.56	216.71	239.94	253.10
	TVR + f_r		377.44	133.71	173.30	206.52	220.74	244.04	257.22
	lit. + IR	−1305.41 ± 14.39	382.42	130.73	165.69	196.03	209.71	232.14	243.98
$O{=}Si(OCH_3)_2$	TVR		347.72	99.19	137.53	179.36	198.10	226.74	241.26
	IR		29.61	10.15	9.01	8.59	8.49	8.39	8.36
	TVR + IR		377.33	109.34	146.54	187.95	206.60	235.14	249.62
	TVR + f_r		378.83	115.58	154.07	195.96	214.71	243.36	257.89
	lit. + IR	−735.55 ± 27.32	378.32	109.72	148.94	190.54	208.82	235.49	247.90
$O{=}Si(OH)(OCH_3)$	TVR		320.20	87.20	115.86	142.99	154.67	172.80	182.36
	IR		14.81	5.06	4.50	4.29	4.25	4.20	4.18
	TVR + IR		335.01	92.27	120.36	147.29	158.92	177.00	186.54
	TVR + f_r		335.96	95.40	124.13	151.29	162.98	181.11	190.67
	lit. + IR	−772.78 ± 26.82	335.43	93.09	120.36	149.91	160.46	175.54	182.91
$Si(OH)_2(OCH_3)_2$	TVR		397.20	137.06	186.40	234.56	255.95	289.85	307.97
	IR		30.11	9.44	8.73	8.48	8.42	8.36	8.34
	TVR + IR		427.31	146.50	195.14	243.04	264.37	298.21	316.31
	TVR + f_r		429.52	153.48	202.96	251.16	272.56	306.47	324.60
	lit. + IR	−1259.38 ± 15.31	430.12	145.35	189.61	235.40	256.29	289.28	306.62
$Si^\bullet(OH)_2(OCH_3)$	TVR		343.25	102.72	133.41	160.96	173.06	192.80	203.76
	IR		14.80	5.04	4.49	4.29	4.24	4.20	4.18
	TVR + IR		358.05	107.76	137.90	165.25	177.30	196.99	207.94
	TVR + f_r		359.45	110.93	141.68	169.26	181.37	201.11	212.07
	lit. + IR	−740.99 ± 4.23	367.61	106.73	132.24	156.93	168.36	187.11	197.37
$Si^\bullet(OH)(OCH_3)_2$	TVR		370.01	112.96	154.17	197.00	216.34	246.75	262.71
	IR		30.10	9.44	8.73	8.48	8.42	8.36	8.34
	TVR + IR		400.12	122.40	162.91	205.48	224.76	255.11	271.05
	TVR + f_r		402.03	129.38	170.72	213.60	232.95	263.37	279.34
	lit. + IR	−706.68 ± 4.35	409.11	124.93	161.93	200.88	218.81	246.97	261.55

[a] TVR is the sum of contributions from translational, vibrational, and external rotation partition functions excluding the vibrational modes which correspond to internal rotation. IR is the sum of contributions from internal rotation partition functions. f_r is the sum of the contribution from vibrational partition functions for the frequencies which corresponds to the internal rotation. lit. is the literature values from online gas-phase resources provided by HiTempThermo, Sandia National Laboratories.

1.76−1.84 and 1.84−1.92 kJ/mol at the same calculation levels. The reason for this difference is probably that the rotor interacts with the adjacent oxygen atom. However, these methyl rotors about the C−O bond are relatively, small and the free rotor approximation may be sufficient, especially in the high-temperature regime, for calculating the thermodynamic properties, that is, the estimated difference between free and classical hindered rotor treatments on the values of C_p is less than 0.03 J/mol per CH_3−O rotor for temperatures above 1000 K.

In this work, the difference between the torsional barriers as calculated using the B3LYP and B97-1 functionals is less than 0.08 kJ/mol for the CH_3 rotor and less than 0.3 kJ/mol for the SiH_3 rotor. Further studies on coupling between rotors in TEOS and TMOS are performed using both B3LYP and B97-1 functionals by calculating the torsional potential of one rotor while keeping another methyl rotor at its highest-energy torsion. The coupled torsional potential is only 0.0004 kJ/mol higher for TEOS and is about 0.005 kJ/mol higher for TMOS. Given

that these rotor−rotor potential couplings are very small, neglecting these potential coupling terms in the partition function for all species seems to be a reasonable choice. Instead, the physical coupling will be taken into account by the effective reduced moment of inertia calculated using Pitzer's formula. In Table 2, several levels of coupled reduced moments of inertia for symmetrical tops are reported.

However, for a molecule containing the heavy Si atom, such a high level $n = 4$ of accuracy does not yield a significant improvement to the thermodynamic properties.

Thermochemistry Calculation. Table 3 contains the important thermodynamic properties for a few important species in the system, as calculated using the B97-1/6-311+G(d,p) frequencies. Enthalpies of formation $\Delta_f H^\circ_{298.15K}$ calculated from isodesmic reactions are also reported in Table 3. The enthalpies in the NIST database are known experimentally with high accuracy, and those by Ho et al. have been computed using high-level MP4 quantum chemistry calculations. The values of Ho et al. compare favorably to the NIST values for small SiH species, within an accuracy range of ±0.01 kJ/mol for S and ±0.3 J/mol for C_p. There are no experimental values available for the larger species, but it is natural to assume that errors will increase, at least linearly, with size. For the complete list of thermodynamic values for all species, please refer to the Supporting Information.

Due to the large number of species that are available in the literature, there are always a number of entirely isodesmic reactions available for each species. The $\Delta_f H^\circ_{298.15K}$ values calculated using isodesmic reactions therefore have an associated error range that can be estimated by the spread of values generated using different reactions. The standard deviation for all of the species that we looked at was between 5 and 40 kJ/mol. The value for $\Delta_f H^\circ_{298.15K}$ that we report is then the mean from all possible isodesmic reactions. This error must be either due to inconsistency in the $\Delta_f H^\circ_{298.15K}$ values presented by Ho and Melius or due to inherent errors in DFT. There is currently no way to determine exactly which is more significant. However, given the strong agreement in other systems with purely experimental values,[20] it is sensible to suppose that there is some significant error associated with the values in ref 10 as calculated using BAC.

Performing a brute force sensitivity analysis with respect to the calculated $\Delta_f H^\circ_{298.15K}$ values, accounting for their respective maximum errors, reveals they have little effect on the equilibrium composition, confirming that these errors are within the acceptable range of accuracy required for postprocessing calculations. This is expected since at high-temperature entropy dominates the Gibbs energy.

For those species that do not have internal rotors, that is, SiH_4 and $SiH_3(O^\bullet)$, Calculated C_p values are extremely precise compared to Ho and Melius's MP4 calculations, with a small underprediction of less than 0.6 J/mol. As soon as a species contains a OH group (the unsymmetrical OH rotor is not treated in this work), such as $O{=}Si(O^\bullet)(OH)$, $Si(O^\bullet)(OH)_3$, $Si(OH)_4$, and so forth, our predicted C_p is less than that of Ho and Melius by 3.2 J/mol per OH group (at 2000 K). However, at temperatures around 300 K, the pure harmonic oscillator treatment agrees very well with Ho and Melius in all cases. This vibrational partition is a good approximation for the OH rotor at low temperatures, but at temperatures above 1000 K, it begins to break down.

For species such as $O{=}Si(OCH_3)_2$, with a CH_3 rotor, the TVR + IR approximation values for C_p are 0.5 J/mol closer to the Ho and Melius ones than those using the TVR + f_r approximation. Treating the CH_3 group as a rotor improves the results significantly.

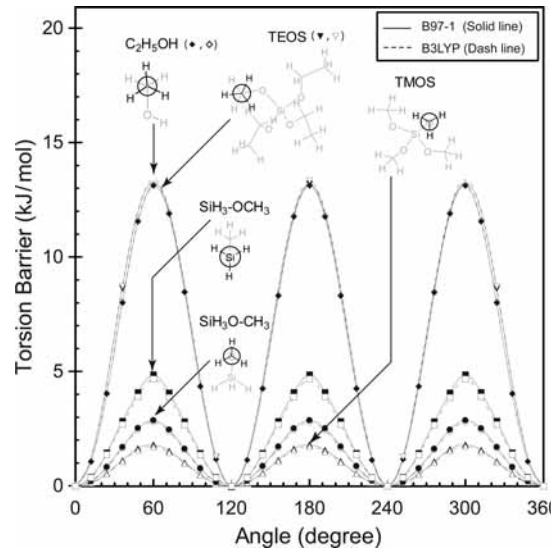

Figure 2. Torsion barrier of the CH_3 and SiH_3 rotors of C_2H_5OH (*trans*-ethanol), SiH_3OCH_3, $Si(OCH_3)_4$, and $Si(OC_2H_5)_4$ calculated at the B97-1/6-311+G(d,p) and B3LYP/6-311+G(d,p) level of theories.

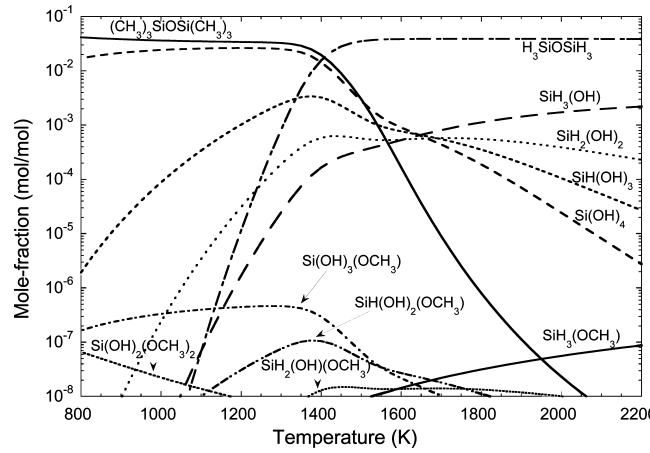

Figure 3. Equilibrium plot showing the gas-phase TEOS system at 1 atm, starting from an initial concentration mixture of TEOS/Ar = 1 mol:1 mol.

Equilibrium Composition. Figure 3 shows the equilibrium composition as a function of temperature. The initial gas mixture used for these simulations comprises 50 mol % TEOS in argon at an atmospheric pressure of 1.01 bar. For clarity, Figure 3 is cut off at a reasonable concentration, removing a large number of the species. A massive number of the species investigated have extremely low concentrations. These may be important to the kinetics as short-lived intermediates. The power of the current methodology is that almost all possible species have been considered, and we can be confident that these species present in high concentration are the species that will be important. Any system involving only manually generated species always faces the risk of failing to spot important stable species, something that becomes more of a certainty than a risk in large complicated chemical systems such as this one.

The most populous species from Figure 3 are $Si(OH)_4$, $SiH(OH)_3$, $SiH_2(OH)_2$, $SiH_3(OH)$, $Si(OH)_3(OCH_3)$, $Si(OH)_2(OCH_3)_2$, the silicon dimers $(CH_3)_3SiOSi(CH_3)_3$ and SiH_3OSiH_3, and the smaller hydrocarbon species CH_4, CO_2, C_2H_4, and C_2H_6. The hydrocarbon species considered are all those hydrocarbons from the ethanol mechanism of Marinov et al.[11] that contain

fewer than two carbon atoms. As expected from basic thermodynamical arguments, the concentrations of nonradical species are almost univerally higher than those for radical species. Though the silicon dimers were not generated automatically as part of this work, they have also been added to the equilibrium calculation, and they appear to be favored over other silicon species, especially SiO_2 between 800 and 1500K. Gas-phase SiO_2 molecules are present at very low concentrations in the temperature range of 500−3500 K and have significant concentrations only at temperatures greater than 4000 K. The high stability of Si dimers in the equilibrium mixture suggests that silica nanoparticles are formed from aggregation of larger gas-phase intermediate species and not directly from SiO_2 as has been suggested.[5] This observation can be validated against experimental evidence where the occurrence of molecular SiO_2 is rare.[42] SiO_2 can only form under certain conditions and not from direct combustion. The intermediate gas-phase silicon-containing dimer species or larger silicon compounds could be made from the silicon-containing radicals derived from those in high concentration mentioned above. These will be necessary for the development of a physically reasonable kinetic model.

The analysis of intermediate species in the system indicates the rapid hydrolysis of the ethyl [$-C_2H_5$] branches from TEOS, confirming the domination of the ethanol mechanism in the Herzler experiment.[5] It can also be seen from the equilibrium calculations that TEOS is highly unstable at high temperatures, with an extremely low concentration of 10^{-23} at 1500 K and 1 atm pressure. The equilibrium graph enables us to identify species that might play an important role in the overall chemical mechanism.

Conclusion

An exhaustive list of 180 $SiO_iC_jH_k$ species involved in the decomposition of TEOS is investigated using quantum chemistry. These calculations are used to obtain thermochemical data, including standard entropies and enthalpies of formation. About 160 of these unique species have not been reported previously in the literature. The presence of internal rotors in the TEOS molecule has also been examined, and their impact on the thermochemistry has been quantified. The new thermochemical data have been utilized to derive equilibrium compositions resulting from the gas-phase decomposition of TEOS at a pressure of 1 atm over a temperature range of 0−2500 K. $Si(OH)_4$, $SiH(OH)_3$, $SiH_2(OH)_2$, $SiH_3(OH)$, $Si(OH)_3(OCH_3)$, $Si(OH)_2(OCH_3)_2$, the silicon dimers $(CH_3)_3SiOSi(CH_3)_3$ and SiH_3OSiH_3, and the smaller hydrocarbon species CH_4, CO_2, C_2H_4, and C_2H_6 are highlighted as the important species. The short-lived radical species, while not present in significant amounts at equilibrium, are likely to be important as intermediates in reactions. This detailed thermochemistry data, along with the analysis of the equilibrium composition, provides a basis for the development of a detailed kinetic model for the decomposition of tetraethoxysilane. Furthermore, the methodology development presented in this work is part of the movement toward full automation of kinetic model development.

Acknowledgment. The authors thank HeiQ materials for funding this work, as well as the Development and Promotion of Science and Technology Talents Project, The Cambridge Commonwealth Trust, and TiOxide Europe Limited for providing financial support to W.P., S.S., and R.S., respectively, and to the EPSRC for help in the form of research hopping Grant Number EP/E01724X-1.

Supporting Information Available: Thermochemistry in the form of NASA polynomial coefficients for all of the species. The Gaussian output files and geometries in the mol format for all of these species. This material is available free of charge via the Internet at http://pubs.acs.org.

References and Notes

(1) Iler, R. K. *The chemistry of silica: solubility, polymerization, colloid and surface properties and biochemistry of silica*; Wiley: Toronto, Canada, 1979.

(2) Slowing, I. I.; Trewyn, B. G.; Giri, S.; Lin, V. S.-Y. *Adv. Funct. Mater.* **2007**, *17*, 1225–1236.

(3) Park, S. K.; Kim, K. D.; Kim, H. T. *Colloid Surf., A* **2002**, *197*, 7–17.

(4) Chu, J. C.; Breslin, J.; Wang, N.; Lin, M. *Mater. Lett.* **1991**, *12*, 179–184.

(5) Herzler, J.; Manion, J. A.; Tsang, W. *J. Phys. Chem. A* **1997**, *101*, 5500–5508.

(6) Morgan, N.; Wells, C.; Kraft, M.; Wagner, W. *Combust. Theory Model.* **2005**, *9*, 449–461.

(7) Wells, C. G.; Morgan, N. M.; Kraft, M.; Wagner, W. *Chem. Eng. Sci.* **2006**, *61*, 158–166.

(8) Morgan, N. M.; Wells, C. G.; Goodson, M. J.; Kraft, M.; Wagner, W. *J. Comput. Phys.* **2006**, *211*, 638–658.

(9) Sander, M.; West, R. H.; Celnik, M. S.; Kraft, M. *Aerosol Sci. Technol.* **2009**, *43*, 1–12.

(10) Ho, P.; Melius, C. F. *J. Phys. Chem.* **1995**, *99*, 2166–2176.

(11) Marinov, N. M. *Int. J. Chem. Kinet.* **1999**, *31*, 183–220.

(12) O'Boyle, N.; Morley, C.; Hutchison, G. *Chem. Cent. J.* **2008**, *2*, 5.

(13) Guha, R.; Howard, M. T.; Hutchison, G. R.; Murray-Rust, P.; Rzepa, H.; Steinbeck, C.; Wegner, J.; Willighagen, E. L. *J. Chem. Inf. Model.* **2006**, *46*, 991–998.

(14) Frisch, M. J.; Trucks, G. W.; Schlegel, H. B.; Scuseria, G. E.; Robb, M. A.; Cheeseman, J. R.; Montgomery, J. A., Jr.; Vreven, T.; Kudin, K. N.; Burant, J. C.; Millam, J. M.; Iyengar, S. S.; Tomasi, J.; Barone, V.; Mennucci, B.; Cossi, M.; Scalmani, G.; Rega, N.; Petersson, G. A.; Nakatsuji, H.; Hada, M.; Ehara, M.; Toyota, K.; Fukuda, R.; Hasegawa, J.; Ishida, M.; Nakajima, T.; Honda, Y.; Kitao, O.; Nakai, H.; Klene, M.; Li, X.; Knox, J. E.; Hratchian, H. P.; Cross, J. B.; Bakken, V.; Adamo, C.; Jaramillo, J.; Gomperts, R.; Stratmann, R. E.; Yazyev, O.; Austin, A. J.; Cammi, R.; Pomelli, C.; Ochterski, J. W.; Ayala, P. Y.; Morokuma, K.; Voth, G. A.; Salvador, P.; Dannenberg, J. J.; Zakrzewski, V. G.; Dapprich, S.; Daniels, A. D.; Strain, M. C.; Farkas, O.; Malick, D. K.; Rabuck, A. D.; Raghavachari, K.; Foresman, J. B.; Ortiz, J. V.; Cui, Q.; Baboul, A. G.; Clifford, S.; Cioslowski, J.; Stefanov, B. B.; Liu, G.; Liashenko, A.; Piskorz, P.; Komaromi, I.; Martin, R. L.; Fox, D. J.; Keith, T.; Al-Laham, M. A.; Peng, C. Y.; Nanayakkara, A.; Challacombe, M.; Gill, P. M. W.; Johnson, B.; Chen, W.; Wong, M. W.; Gonzalez, C.; Pople, J. A. *Gaussian 03*, revision C.02; Gaussian, Inc.: Wallingford, CT, 2004.

(15) Becke, A. D. *J. Chem. Phys.* **1993**, *98*, 5648–5652.

(16) Becke, A. D. *J. Chem. Phys.* **1997**, *107*, 8554–8560.

(17) Krishnan, R.; Binkley, J. S.; Seeger, R.; Pople, J. A. *J. Chem. Phys.* **1980**, *72*, 650–654.

(18) McLean, A. D.; Chandler, G. S. *J. Chem. Phys.* **1980**, *72*, 5639–5648.

(19) Boese, A. D.; Martin, J. M. L.; Handy, N. C. *J. Chem. Phys.* **2003**, *119*, 3005–3014.

(20) West, R. H.; Beran, G. J. O.; Green, W. H.; Kraft, M. *J. Phys. Chem. A* **2007**, *111*, 3560–3565.

(21) Lee, C.; Yang, W.; Parr, R. G. *Phys. Rev. B* **1988**, *37*, 785–789.

(22) Hamprecht, F. A.; Cohen, A. J.; Tozer, D. J.; Handy, N. C. *J. Chem. Phys.* **1998**, *109*, 6264–6271.

(23) Wilson, P. J.; Tozer, D. J. *Chem. Phys. Lett.* **2002**, *352*, 540–544.

(24) Pfaendtner, J.; Yu, X.; Broadbelt, L. J. *Theor. Chem. Acc.* **2007**, *118*, 881–898.

(25) da Silva, G.; Kim, C.-H.; Bozzelli, J. W. *J. Phys. Chem. A* **2006**, *110*, 7925–7934.

(26) Sumathi, R.; Carstensen, H.-H.; Green, W. H. *J. Phys. Chem. A* **2001**, *105*, 6910–6925.

(27) Speybroeck, V. V.; Vansteenkiste, P.; Neck, D. V.; Waroquier, M. *Chem. Phys. Lett.* **2005**, *402*, 479–484.

(28) Pitzer, K. S.; Gwinn, W. D. *J. Chem. Phys.* **1942**, *10*, 428–440.

(29) East, A. L. L.; Radom, L. *J. Chem. Phys.* **1997**, *106*, 6655–6674.

(30) McClurg, R. B.; Flagan, R. C.; Goddard, W. A., III. *J. Chem. Phys.* **1997**, *106*, 6675–6680.

(31) Manion, J. A.; et al. *NIST Chemical Kinetics Database, NIST Standard Reference Database 17*, version 7.0 (web version), release 1.4.2, data version 2008.12; National Institute of Standards and Technology: Gaithersburg, MD, 2008; http://kinetics.nist.gov/.

(32) Melius, C. F. In *Chemistry and physics of energetic materials*; Bulusu S. N., Ed.; Kluwer Academic Pub. (Springer): Norwell, MA, 1990; Vol. 301, pp 21−49.

(33) Pedley, J. B.; Naylor, R. D.; Kirby, S. P. *Thermochemical data of organic compounds*; Chapman and Hall: New York, 1986.

(34) Cox, J. D.; Wagman, D. D.; Medvedev, V. A. *CODATA Key Values for Thermodynamics*; Hemisphere Publishing Corp.: New York, 1989.

(35) Allendorf, M. D.; Melius, C. F.; Ho, P.; Zachariah, M. R. *J. Phys. Chem.* **1995**, *99*, 15285–15293.

(36) Goodwin, D. G. *An open-source, extensible software suite for CVD process simulation*, Technical Report; The Electrochemical Society (http://www.electrochem.org/), 2003.

(37) Gordon, S.; McBride, B. J. *Computer program for calculation of complex chemical equilibrium composition, rocket performance, incident and reflected shocks and chapman-jouget detonations*, Technical Report; NASA, 1976.

(38) Kee, R. J.; Ropley, F. M.; Meeks, E.; Miller, J. A. *CHEMKIN-III: A FORTRAN chemical kinetics package for the analysis of gas-phase chemical and plasma kinetics*, Technical Report UC-405 SAND96-8216, Sandia Labs (http://public.ca.sandia.gov/casite/index.php), 1996.

(39) Chao, J.; Hall, K. R. *Int. J. Thermophys.* **1986**, *7*, 431–442.

(40) Durig, J. R.; Bucy, W. E.; Wurrey, C. J.; Carreira, L. A. *J. Phys. Chem.* **1975**, *79*, 988–993.

(41) Viruela, P. M.; Viruela, R.; Orti, E.; Bredas, J.-L. *J. Am. Chem. Soc.* **1997**, *119*, 1360–1369.

(42) Jutzi, P.; Schubert, U. *Silicon chemistry: from the atom to extended systems*; Wiley-VCH: Bielefeld, Germany, 2003.

JP905494S